ACS APPLIED MATERIALS & INTERFACES

www.acsami.org

Research Article

Polydimethylsiloxane Polymerized Emulsions for Acoustic Materials Prepared Using Reactive Triblock Copolymer Surfactants

Tucker J. McKenzie, Thomas Brunet, Lyndsay N. Kissell, Pietro Strobbia, and Neil Ayres*

Cite This: *ACS Appl. Mater. Interfaces* 2023, 15, 58917−58930

Read Online

ACCESS | Metrics & More | Article Recommendations | Supporting Information

ABSTRACT: Porous polymers have interesting acoustic properties including wave dampening and acoustic impedance matching and may be used in numerous acoustic applications, e.g., waveguiding or acoustic cloaking. These materials can be prepared by the inclusion of gas-filled voids, or pores, within an elastic polymer network; therefore, porous polymers that have controlled porosity values and a wide range of possible mechanical properties are needed, as these are key factors that impact the sound-dampening properties. Here, the synthesis of acoustic materials with varying porosities and mechanical properties that could be controlled independent of the pore morphology using emulsion-templated polymerizations is described. Polydimethylsiloxane-based ABA triblock copolymer surfactants were prepared using reversible addition−fragmentation chain transfer polymerizations to control the emulsion template and act as an additional cross-linker in the polymerization. Acoustic materials prepared with reactive surfactants possessed a storage modulus of ∼300 kPa at a total porosity of 71% compared to materials prepared using analogous nonreactive surfactants that possessed storage modulus values of ∼150 kPa at similar porosities. These materials display very low longitudinal sound speeds of ∼35 m/s at ultrasonic frequencies, making them excellent candidates in the preparation of acoustic devices such as metasurfaces or lenses.

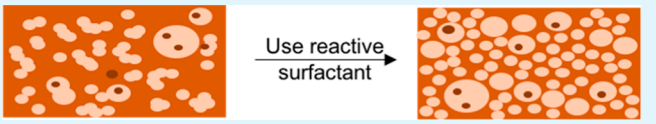

KEYWORDS: *emulsion templated polymerization, reactive surfactants, acoustic materials, polyHIPE, block copolymers*

INTRODUCTION

Acoustic materials possess properties including wave dampening,[1,2] wave guiding,[3] and acoustic impedance matching,[4−6] which enable their use in applications including acoustic cloaks[7,8] and metamaterial devices.[9,10] Many of these acoustic materials, including the first reported locally resonant acoustic polymer material by Sheng and co-workers,[11] are composites consisting of a polymer matrix with a filler, such as metallic particles, which acts as scatterers or resonators. While acoustic materials have been prepared from polymer-based composites that obtain rapid, on-demand changes in the frequency range for acoustic wave blocking or guiding in a single material,[12,13] these can require advanced fabrication techniques, and the preparation of the final device can rely on multistep manufacturing processes, making them costly or difficult to prepare.[9,10]

Acoustic materials can be prepared without metal scatters or resonators by using gas-filled voids within an elastic polymer matrix. It has been established that in these materials, the longitudinal sound speed (C_L) depends on the void density (i.e., porosity) and stiffness of the material.[14−17] Specifically, porous elastomers that are dense and compressible can reduce C_L while porous, rigid polymers show little impact on C_L at comparable porosity values. For example, C_L values of ∼50 m/s were observed during ultrasonic acoustic analysis of a soft, porous polydimethylsiloxane (PDMS)-based material with a storage modulus of ∼0.29 MPa while a stiffer polystyrene/divinylbenzene network porous material with a storage modulus of ∼1.2 GPa obtained C_L values of ∼1050 m/s, although both materials possessed similar porosities of ∼30%.[18] The porosity of PDMS appears to have an effect on C_L, where a sudden drop of C_L was observed with increasing porosity before a plateauing in the values observed over a porosity range of 0−35% porosity.[17] Porous polysiloxanes have now been widely reported as acoustic materials,[18−25] but there remains a need for the development of porous siloxanes that can obtain a wide range of porosities, especially at higher porosities, and mechanical properties to access materials with new properties for acoustic lenses and metasurfaces. Acoustic metasurfaces consist of a single material with a subwavelength thickness that has a gradient of distinctly different acoustic properties, e.g., acoustic index, to act as a lens to focus or shape acoustic waves, and this can be achieved by producing gradients of stiffness or porosity using polymer-based acoustic metasurfaces.[26] The design and preparation of such subwavelength materials are important in obtaining novel devices for applications in metamaterials, acoustic cloaks, and underwater impedance matching.[10]

Received: October 12, 2023
Revised: November 26, 2023
Accepted: November 28, 2023
Published: December 8, 2023

One method to prepare porous PDMSs with controlled porosity values is the emulsion templating technique known as polymerized high internal phase emulsions (polyHIPEs).[27−30] PolyHIPEs are prepared using an emulsion of an internal phase (IP), typically water, stabilized within a polymerizable continuous phase (CP) using surfactants or amphiphilic particles.[31−33] The CP is polymerized, and the IP is removed to yield a porous material. Importantly, this emulsion templating approach can result in materials possessing a wide range of total porosity values of lower than 10% to over 95%, and this value can be controlled by adjusting the initial volume fraction of the IP in the precursor emulsion. In this regard, emulsion-templated polymerizations are conventionally named with respect to their volume fraction of the IP. Specifically, emulsions consisting of an IP volume fraction >74% are called polyHIPEs, while emulsions having an IP volume fraction between 74 and 25% are called medium internal phase emulsions (polyMIPEs), and emulsions with <24% IP are called low internal phase emulsions (polyLIPEs), respectively. Emulsion-templated polymers made using low glass-transition temperature elastomers, including PDMS can suffer from collapse of the pore structure at porosity values over ∼60%.[34,35] Methods such as the use of super critical CO_2 drying or the addition of internal blowing agents such as peroxides have used to try to overcome this challenge,[19,20,25] and recently our group has shown that increasing the cross-linking density of the PDMS network is a simple route to achieve polyHIPEs having a porosity of 77% under standard drying conditions and without additives.[28]

The pore morphology of porous polymer materials can play a significant role in the materials' mechanical properties.[36−38] Specifically, pore size, pore wall thickness, strut thickness, and pore interconnectivity or "degree of openness" are all factors that have an impact on mechanical properties of porous polymer materials.[39,40] The degree of openness is used to quantify the relationship between open and closed pores, and in general, the higher the degree of openness, the lower the mechanical properties. Pore morphology in polyHIPEs can be controlled by two main factors, the type and concentration of stabilizer (i.e., the surfactant or amphiphilic particle) and the locus of initiation of the polymerization.[41−45] In general, closed-cell pore structures can be obtained during particle-stabilized Pickering emulsions or by initiating the polymerization from within the IP of the emulsion. Alternatively, open-cell pore structures can be obtained by using polymeric surfactants and by initiating the polymerization from the CP. Furthermore, tuning of the pore structure has been achieved using block copolymer surfactants with different ratios of hydrophilic to hydrophobic character.[46,47] One method to prepare amphiphilic block copolymer surfactants is reversible addition−fragmentation chain transfer (RAFT) polymerizations,[48,49] and this method has been used to prepare surfactants for HIPE stabilization.[50−52] For example, Debuigne and co-workers[53] synthesized a library of poly(ethylene oxide)/polystyrene (PEO/PS) block copolymers with different PS contents using RAFT polymerizations to prepare PS/DVB-based polyHIPEs with different degrees of openness. In that work, it was shown that PEO/PS surfactants with equal block ratios obtained the highest degree of openness of ∼10%, and surfactants with the highest PS content obtained the lowest degree of openness of ∼2%. Polymeric surfactants change the properties of polyHIPEs' pore surfaces by introducing functionality into the polyHIPE surface from the surfactant.[52,54−59] When these types of surfactants are integrated into the polymer network through physical anchoring or chemical reactions during the polymerization of the CP of the polyHIPE, they are called "reactive" surfactants. Reactive surfactants have been used to limit surfactant leaching[54] or introduce hydrophilicity to a hydrophobic polymer surface in a one-step process,[55] and they have recently been shown to improve the compressive mechanical properties of polyHIPEs compared to small-molecule surfactants.[46]

Previously, we reported PDMS-based acoustic materials prepared from thiol- and ene-functionalized PDMSs using polymerized emulsion templating methods that obtain low C_L values of ∼40−50 m/s.[23,35] In these reports, the thiol to ene ratio was varied to adjust the mechanical properties, and we were able to obtain materials with moduli differences of ∼200 kPa at a single porosity. We used the commercially available surfactant "Silube" to stabilize the emulsions in our previous work, and we were consequently limited to a single pore morphology in the final polymerized materials. Herein, we describe the synthesis of a set of reactive and nonreactive PDMS-based ABA triblock copolymer surfactants using RAFT polymerizations, with the aim of controlling the emulsion morphology of the precursor template to prepare porous PDMSs with improved acoustic properties in reducing C_L sound speeds. The reactive surfactants serve as an additional cross-linker at the interface of the IP and CP by participating in thiol−ene reactions during the polymerization of the emulsions.

EXPERIMENTAL SECTION

Materials. The reagents amino-2-propanol, methacrylic anhydride, potassium ethyl xanthogenate, 2-bromoethanol, acryloyl chloride, 1-dodecanethiol, Aliquot 336, carbon disulfide, *N*,*N*′-dicyclohexylcarbodiimide (DCC), 4-dimethylaminopyridine (DMAP), *n*-tributylphosphine, 2,2-dimethoxy-2-phenylacetophenone (DMPA), 2,2′-azobis(2-methylpropionitrile) (AIBN) and benzoyl peroxide (BPO), and reagent grade solvents dichloromethane (DCM), tetrahydrofuran (THF), methanol (MeOH), acetone, and chloroform, and *N*,*N*′-dimethylacrylamide (DMA) monomer were purchased from Sigma-Aldrich (St. Louis, MO, USA). The polymers [13−17% (mercaptopropyl) methylsiloxane]−dimethylsiloxane copolymer (thiolated-PDMS), vinyl terminated polydimethylsiloxane (vinyl-PDMS), hydroxy-terminated PDMS (10,000 g/mol), and (30−35% dodecylmethylsiloxane)−[7−10% hydroxy(propethyleneoxy (6−9) propyl) methylsiloxane]−(55−65% dimethylsiloxane) terpolymer (Silube J208-812) were purchased from Gelest (Morrisville, PA, USA). Sodium chloride (NaCl), sodium hydroxide (NaOH), hydrochloric acid (HCl), sodium sulfate, and diethyl ether were purchased from Oakwood Chemical (Estill, SC, USA). Ultra-Pure Milli-Q water was obtained from an in-house purification system. All reagents and chemicals were used as received, unless stated otherwise. The DMA monomer was passed through an alumina column to remove the inhibitor and stored in the refrigerator before use; AIBN and BPO were precipitated twice and stored in the freezer before use.

Methods. *Synthesis of 2-Hydroxypropyl Methacrylamide.* Amino-2-propanol (20.0 g, 266 mmol) was dissolved in 200 mL of a diethyl ether/DCM solution (25:1 vol/vol) in a flame-dried round-bottom flask equipped with a stir bar. Methacrylic anhydride (40.0 g, 260 mmol) was dissolved in 200 mL of diethyl ether, and then this solution was added dropwise to the reaction vessel using an addition funnel that was fixed to the round-bottom flask. The reaction was allowed to proceed for 4 h at room temperature before being cooled to −20 °C for 12 h to obtain the crystallized crude product as a white solid. The solids were obtained by vacuum filtration, recrystallized from a diethyl ether/DCM mixture (4:1 vol/vol), and collected using vacuum filtration to yield 29.8 g (∼80%) product as a crystalline white

https://doi.org/10.1021/acsami.3c14859
ACS Appl. Mater. Interfaces 2023, 15, 58917−58930

solid. ^{1}H NMR (400 MHz, $CDCl_3$): δ [ppm] = 6.55 (s, 1H; NH), 5.74 (s, 1H; CCH_2 vinyl), 5.35 (s, 1H; CCH_2 vinyl), 3.94 (s, 1H; OH), 3.48 (m, 2H; CH_2), 3.17 (m, 1H; CH) 1.97 (s, 3H; CH_3), 1.19 (t, 3H; CH3) ^{13}C NMR (101 MHz, $CDCl_3$): δ 169.48 (C═O), 139.60 (C═C), 120.14 (C═C), 67.29, 47.17, 20.97, 18.67 (Figure S1).

Synthesis of S-2-Hydroxyethyl-O-ethyl Dithiocarbonate. This compound was synthesized following a protocol modified from previous literature reports.[60,61] Potassium ethyl xanthogenate (26.9 g, 168 mmol) was dissolved in 105 mL of acetone in a flame-dried round-bottom flask equipped with a stir bar and an addition funnel. Separately, 2-bromoethanol (17.25 g, 138 mmol) was dissolved in 45 mL of acetone, and this solution was added dropwise to the reaction mixture over the course of 1 h. The reaction was allowed to proceed for 12 h at room temperature. The solids were removed by using vacuum filtration and extensively washed with acetone to obtain a slightly yellow solution. The solution was concentrated by using a rotary evaporator to obtain a yellow solid. The solid was dissolved in chloroform, washed three times with brine, dried over sodium sulfate, and concentrated to dryness using a rotary evaporator to yield 21.8 g (~95%) of a yellow liquid. ^{1}H NMR (400 MHz, $CDCl_3$): δ [ppm] = 4.59 (2H, q, CH_2CH_3), 3.85 (2H, t, $OHCH_2CH_2$), 3.34 (2H, t, CH_2CH_2S), 3.19 (1H, br s, OH), 1.43 (3H, t, CH_2CH_3) ^{13}C NMR (101 MHz, $CDCl_3$): δ 214.54, 70.33, 60.49, 38.26, 13.83 (Figure S2).

Synthesis of a Xanthate-Containing Monomer. The ethyl xanthate acrylate (EXA) monomer was synthesized following a protocol modified from previous literature reports.[60,61] *S*-2-Hydroxyethyl-*O*-ethyl dithiocarbonate (8.3 g, 50 mmol) and triethyl amine (9.2 g, 65 mmol) were dissolved in 60 mL of anhydrous DCM in a flame-dried round-bottom flask equipped with a stir bar and an addition funnel. The reaction mixture was placed in an ice-water bath to cool for 30 min before a solution of acryloyl chloride (12.2 mL, 125 mmol) in 30 mL of DCM was added dropwise over the course of 1 h. The reaction was allowed to proceed for 12 h at room temperature. Excess acryloyl chloride was quenched by the addition of ~15 mL of water while the reaction was stirring. The mixture was transferred to a separatory funnel and washed with water three times, 0.5 M solution of HCl three times, 0.5 M solution of NaOH three times, and once with brine. The organic layer was collected, dried over sodium sulfate, passed through a column of neutral alumina, and concentrated with a rotary evaporator to yield 9.2 g (~79%) of a yellow liquid. ^{1}H NMR (400 MHz, $CDCl_3$): δ [ppm] = 6.41, 6.14, and 5.86 (m, 3H; $CHCH_2$ vinyl), 4.65 (q, 2H; CH_2), 4.40 (t, 2H; CH_2), 3.44 (t, 2H; CH_2), 1.44 (t, 3H; CH_3) ^{13}C NMR (101 MHz, $CDCl_3$): δ 213.53 (C═S), 155.75 (C═O), 131.45 (C═C), 127.97 (C═C), 70.38, 62.02, 34.24, 13.79 (Figure S3).

Synthesis of 2-(Dodecylthiocarbonothioylthio)-2-methylpropionic Acid. The chain transfer agent (CTA) DDMAT was synthesized following a modified protocol from a previous report.[62] 1-Dodecanethiol (44.14 mL, 184 mmol) and 3.38 Aliquot 336 (3.38 mL, 7.4 mmol) were dissolved in 110 mL of acetone in a 1 L three-neck round-bottom flask equipped with a stir bar and addition funnel. The reaction vessel was sealed using a rubber septum and placed into an ice-water bath, and the reaction solution was bubbled gently with nitrogen for 15 min. While under a nitrogen atmosphere, a solution of NaOH (15.5 g, 50 wt %) was added to the reaction mixture dropwise using the addition funnel while vigorously stirring and allowed to further proceed for 15 min before a solution of carbon disulfide (11.1 mL, 184 mmol) in 25 mL of acetone was added dropwise through the addition funnel. The reaction mixture was allowed to further stir for 15 min. Chloroform (22.3 mL, 275 mmol) was added to the reaction vessel in one portion while the solution was stirring. A second portion of a NaOH solution (73.7 g, 50 wt %) was added dropwise to the reaction mixture, and the reaction was allowed to proceed for 12 h at room temperature. While stirring, 300 mL of water was added to the reaction vessel and a glass rod was used to gently break up large portions of a precipitate that was formed. The solution was then acidified with concentrated HCl to a pH of ~3 at which point a biphasic solution of a red organic layer and yellow aqueous solution was obtained. The solution was further acidified using concentrated HCl until the red organic layer was fully precipitated. The solids were collected using vacuum filtration and suspended in ~500 mL of methanol while stirring to wash the precipitate. The solids were removed using vacuum filtration, the organic layer was concentrated to a red viscous oil using rotary evaporation, and the crude product was recrystallized twice from hexane to yield 16.2 g (~24%) of a yellow crystalline product. ^{1}H NMR (400 MHz, $CDCl_3$): δ [ppm] = 11.19 (s, 1H; COOH), 3.28 (t, 2H; CH_2), 1.72−1.67 (m, 8H; $C(CH_3)_2$ and SCH_2CH_2), 1.38−1.25 (m, 18H; $CH_2(CH_2)_9CH_3$), 0.88 (t, 3H; CH_3) ^{13}C NMR (101 MHz, $CDCl_3$): δ 220.76 (C═S), 179.35 (C═O), 55.72, 37.05, 31.94, 29.67, 29.66, 29.60, 29.49, 29.38, 29.15, 29.01, 27.84, 25.23, 22.72, 14.17 (Figure S4).

Synthesis of DDMAT-Terminated PDMS Macro-CTA. PDMS mCTA was synthesized following a modified protocol from a previous literature report.[63] Hydroxy-terminated PDMS (20.0 g, 2 mmol, 10,000 g/mol), DDMAT (1.83 g, 5 mmol), and DMAP (98 mg, 0.8 mmol) were dissolved in 150 mL of anhydrous DCM in a flame-dried round-bottom flask equipped with a stir bar. A solution of DCC (1.65 g, 8 mmol) in 50 mL of anhydrous DCM was added to the reaction mixture, the round-bottom flask was sealed with a septum, and the reaction mixture was transferred to an oil bath preheated to 40 °C and allowed to stir for 24 h. The reaction was cooled to room temperature before the solids were removed using vacuum filtration, and the organic layer was collected and then concentrated under rotary evaporation to yield a viscous yellow oil. The crude product was dissolved in 300 mL of hexane and filtered to remove any remaining solids. The hexane solution was then washed three times with 50 mL portions of methanol to remove unreacted DDMAT. The hexane layer was then washed extensively with water and then brine, dried over sodium sulfate, and concentrated using a rotary evaporator to yield a yellow oil. The yellow oil was then dissolved in DCM and passed through a basic alumina column and concentrated to dryness to yield 19.4 g (~90%) of a yellow oil. ^{1}H NMR (400 MHz, $CDCl_3$) and ^{13}C NMR (101 MHz, $CDCl_3$): δ [ppm] = 220.35 (C═S) and 178.34 (C═O) (Figure S5).

General Protocol for the RAFT Polymerization of PDMS-Based Nonreactive Surfactants. This protocol was followed for the synthesis of ABA triblock copolymer surfactants with hydrophilic blocks consisting of DMA, HPMA, and mPEG monomers. For example, in a general polymerization to obtain a PDMS-DMA surfactant, PDMS mCTA (3 g, 0.27 mmol), DMA (3.74 g, 37.3 mmol), and AIBN (5 mg, 0.03 mmol) were dissolved in 40 mL of a 1:1 toluene/*t*-butanol solution (v/v) in a round-bottom flask equipped with a stir bar and sealed with a rubber septum. The polymerization solution was bubbled with nitrogen for 20 min and then placed in an oil bath preheated to 70 °C and allowed to proceed for 24 h. The polymerization was stopped by exposure to oxygen. A sample was obtained to determine monomer conversion, and the remaining polymerization solution was concentrated to a yellow solid under rotary evaporation. The crude polymer was dissolved in DCM and precipitated from cold methanol twice to yield a yellow solid. ^{1}H NMR spectra have been provided for PDMS-DMA (Figure S6), PDMS-HPMA (Figure S7), and PDMS-mPEG (Figure S8) surfactants and were used to obtain the block ratios by comparison of the ratio of PDMS to the hydrophilic monomer.

General Protocol for the RAFT Polymerization of DMA/EXA PDMS-Based Reactive Surfactants with Protected-Thiol Functionality. This protocol was followed for the synthesis of ABA triblock copolymer surfactants by the copolymerization of DMA and EXA with PDMS mCTA to prepare surfactants having a protected thiol functionality. For example, in a general polymerization, PDMS mCTA (3 g, 0.27 mmol), EXA (2.68 g, 11.5 mmol), DMA (2.67 g, 26.7 mmol), and AIBN (5 mg, 0.03 mmol) were dissolved in 40 mL of a 1:1 toluene/*t*-butanol solution (v/v) in a round-bottom flask equipped with a stir bar and sealed with a rubber septum. The polymerization solution was bubbled with nitrogen for 20 min, then placed in an oil bath preheated to 70 °C, and the reaction was allowed to proceed for 24 h. The polymerization was stopped by exposure to oxygen. A sample was obtained to determine monomer conversion, and the remaining polymerization solution was concentrated to a

https://doi.org/10.1021/acsami.3c14859
ACS Appl. Mater. Interfaces 2023, 15, 58917−58930

yellow solid under rotary evaporation. The crude polymer was dissolved in DCM and precipitated from either methanol or diethyl ether to yield a yellow solid. ^{1}H NMR spectra have been provided for PDMS-DMA/EXA surfactants (Figure S9) and were used to obtain the block ratios by comparison of the ratio of PDMS to either DMA or EXA peaks. The dimethyl peaks (3.2−2.75 ppm) were used for DMA while the methylene peaks (4.65−4.55 ppm) from the ethyl ether group were used for EXA.

General Protocol for CTA End-Group Removal of PDMS-Based Surfactants. The long hydrocarbon chain of DDMAT was removed from the PDMS-based triblock copolymer surfactants using radical termination. In a typical reaction, the CTA-terminated polymer was reacted with AIBN and BPO following a molar ratio of 1:20 (CTA/AIBN) and 10:1 (AIBN/BPO). For example, CTA-terminated PDMS-DMA surfactant (3.0 g, 0.12 mmol), AIBN (0.80 g, 4.8 mmol), and BPO (0.12 g, 0.48 mmol) were dissolved in 60 mL of DMF in a round-bottom flask equipped with a stir bar and sealed with a rubber septum. The reaction vessel was purged with nitrogen, placed into an oil bath preheated to 70 °C, and allowed to proceed for 12 h. The reaction was stopped by exposure to air and cooled to room temperature before being purified by dialysis for 5 days with water bath changes ∼every 12 h. The end-group-removed polymer was isolated under lyophilization to yield a white powder and characterized by ^{13}C NMR (Figure S10), digital imaging, and gel permeation chromatography. A representative digital image showing the color change that was apparent after the end-group removal reaction and the image is presented in Figure S11.

General Protocol for Thiol-Deprotection of DMA/EXA PDMS-Based Surfactants. Deprotection reactions of DMA/EXA PDMS surfactants were performed following previous reports.[60,61] For example, the surfactant $PDMS_{137}$−DMA_{110}/EXA_{66} ($M_{n,th}$ = 30,700; 66 xanthate functional groups per chain) (3.5 g, 7.5 mmol of thiocarbonyl functionality) was dissolved in 25 mL of anhydrous THF in a glass vial equipped with a stir bar, sealed with a rubber septum, and placed under a nitrogen atmosphere. Isopropyl amine (0.53 g, 9 mmol, 20% molar excess with respect to thiocarbonyl functionality) was added to the reaction mixture and allowed to stir for 10 min. 1−2 drops of a dilute solution of *n*-tributylphosphine (*n*TBP) in THF (1 mL *n*TBP in 20 mL THF) was added to the reaction mixture, and the reaction was allowed to proceed for 12 h at room temperature. Note: *n*TBP is a pyrophoric chemical and was used in a glovebox under an argon atmosphere. Within the first hour, the reaction solution became an off-white solution that had started as a bright yellow solution indicating that aminolysis of the xanthate group was occurring. The deprotected polymer was purified by dialysis for 5 days with frequent water bath changes and isolated by lyophilization to yield a white powder that was stored under a nitrogen atmosphere at −20 °C. The final deprotected polymer was characterized by NMR spectroscopy and digital imaging and is presented in Figures S12 and S13, respectively. The loss of the methylene proton peaks in the ^{1}H NMR spectrum (Figure S12) indicates that the deprotection reaction was successful. Additionally, a stark color change of the surfactant from bright yellow to white was observed for the protected and deprotected polymer, respectively, further confirming that the deprotection reaction was successful as the yellow color comes from the thiocarbonyl-containing species (Figure S13).

Preparation of Water-in-PDMS Emulsions Using Silube. MIPEs were prepared using a modified procedure from our lab.[23,24] The continuous phase was first prepared in a 20 mL glass vial. Typically, thiolated-PDMS (0.25 g, 0.285 mmol thiol-functional group), vinyl-PDMS (0.857 g, 0.285 mmol alkene-functional group), and Silube (11 mg, 1.0 wt % with respect to weight of the continuous phase) were combined and vortexed. The dispersed phase (1.72 g, 60% v/v) consisting of a 1.5% w/v NaCl Mili-Q water solution was added in small portions and vortexed until a viscous emulsion formed. The emulsion was characterized by rheology and optical microscopy.

Preparation of Water-in-PDMS Emulsions Using Synthetic Surfactants. The continuous phase was first prepared in a 20 mL glass vial. Typically, thiolated-PDMS (0.25 g, 0.285 mmol of thiol-functional group) and vinyl-PDMS (0.857 g, 0.285 mmol of alkene-functional group) were combined and vortexed. In a separate 20 mL glass vial, the dispersed phase was prepared consisting of the synthetic surfactant (11 mg, 1.0 wt % with respect to weight of the continuous phase) dissolved in 1.5 wt %/vol NaCl Mili-Q water solution (1.72 g, 60% v/v). This dispersed phase containing the surfactant was added in small portions to the continuous phase vial and vortexed until a stable emulsion formed. The emulsion was characterized by rheology and optical microscopy.

Preparation of PolyMIPEs Using Either Silube or Synthetic Surfactants. PolyMIPEs were prepared following their respective emulsion preparation protocols with a slight modification of the preparation of the continuous phase. In all formulations, the photoinitiator DMPA (1.0 wt % with respect to weight of the continuous phase) was dissolved in approximately 0.2 mL of DCM in a small glass vial before being added to the continuous phase. After this polymerizable continuous phase was formed, the dispersed phase was added in small potions. After an emulsion was formed, the emulsion was transferred to a mold and irradiated with UV light (λ_{max} = 365 nm) for 6 min in a mirrored enclosure and allowed to stand further for 5 min before being removed from the mold. PolyMIPEs were placed in the fume hood and dried for ∼48 h at 22 °C. The resulting dried materials were characterized using scanning electron microscopy, density measurements, and dynamic mechanical analysis.

^{1}H and ^{13}C NMR spectroscopy was performed using a Bruker Ultrashield 400 MHz (100 MHz for ^{13}C NMR) instrument, and the data were processed using Mestre Nova 14.3 software. Molecular weights of polymers were determined by gel permeation chromatography according to protocols from our lab[64] using an Agilent 1200 series HPLC equipped with a PSS Gram guard column (10 μm) and two PSS Gram columns (10 μm) with filtered DMF with 0.1% LiBr w/v mobile phase at a flow rate of 0.5 mL/min at 70 °C using an Optilab rEX differential refractometer (light source 658 nm) detector calibrated against poly(styrene) standards (850−2,000,000 Da) and ASTRA software v. 6.1.0 data calculation. Critical micelle concentration values were obtained by surface tension experiments using a surface tensiometer (BZY-102, Shanghai Fangrui Instruments) by the du Nouy ring method (platinum ring, 20 mm diameter). The aqueous solution used for measurements was the 1.5 wt % NaCl solution used for emulsion preparation. The surfactant was added in small increments until a minimum surface tension was observed. The critical micelle concentration (CMC) was recorded as the initial concentration value when the surface tension value remained constant. Optical microscopy images were collected with a Nikon Ti_2 microscope with an S FL 20× objective and NIS Elements software (v5.41.01). The images were processed, and the scale bars were added by using ImageJ 1.53c. For each formulation, a small droplet of the emulsion was placed on to a microscope slide, and images were obtained immediately. Rheology experiments were performed on emulsions following previously reported protocols from our lab[24] using a Discovery Series Hybrid Rheometer (Model HR-2, TA Instruments) using 20 mm diameter parallel plates and controlled temperature using an advanced Peltier system on three replicate emulsions. Oscillatory frequency sweep (0.1−100 Hz; 0.1% strain) and flow sweep (0.1−100 Hz) experiments were performed at room temperature (22 °C) and on emulsions that were prepared immediately before characterization. Average pore morphology observations were obtained by analysis of scanning electron microscopy (SEM) images using a scanning electron microscope (low-vacuum) (FEI XL-30) equipped with an EDAX detector. Cross sections of the materials were cut from dried polyMIPEs or composites from chosen locations and fixed onto aluminum stubs and imaged at an accelerating voltage of 15 kV. Average pore diameter and average pore throat diameter were obtained by measuring the diameter of 100 pores and 50 pore throats from SEM images using ImageJ software. Total porosity calculations and density measurements were obtained from dried polyMIPE samples using a home-built Archimedes balance from three replicates of each formulation following protocols from our lab.[23,24] We calculated the total porosity of the polyMIPEs using eq 1 where ρ is the average density of the bulk

https://doi.org/10.1021/acsami.3c14859
ACS Appl. Mater. Interfaces 2023, 15, 58917−58930

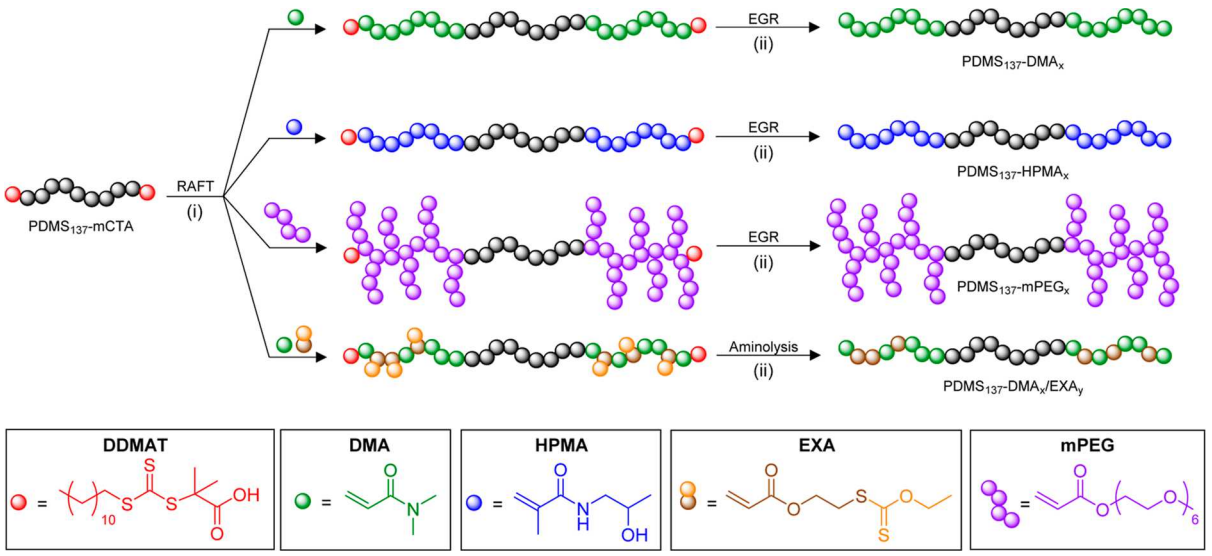

Figure 1. Cartoon overview of the process to obtain ABA triblock copolymer surfactants using RAFT. Triblock copolymers are prepared (i) starting from the DDMAT-terminated PDMS macroCTA that is polymerized with the chosen monomers. In the post polymerization process (ii), AIBN radical termination is used for CTA end group removal (EGR) and aminolysis is used as a thiol deprotection process for xanthate-containing surfactants to obtain the surfactants used to stabilize emulsions. Colored beads are used to represent PDMS (black beads), CTA DDMAT (red beads), and the different monomer repeat units with a key found in the bottom of the figure.

Table 1. Polymer Surfactant Characterization Results[a]

surfactant	surfactant block ratios[b] (PDMS/hydrophilic)	$M_{n,NMR}$[b] (g/mol)	$M_{n,SEC}$[c] (g/mol)	$Đ$[c]	CMC[d] (mg/L)
silube			15,000	2.9	NS
$PDMS_{137}$–mCTA			11,000	1.8	
$PDMS_{137}$–DMA_{271}	1:1.98	38,100	26,000	1.5	210
$PDMS_{137}$–DMA_{138}	1:1.01	24,800	21,000	1.6	145
$PDMS_{137}$–DMA_{71}	1:0.52	18,100	8000	1.3	90
$PDMS_{137}$–$HPMA_{214}$	1:1.56	41,600	44,000	1.4	140
$PDMS_{137}$–$HPMA_{95}$	1:0.69	24,600	39,000	1.5	100
$PDMS_{137}$–$HPMA_{80}$	1:0.58	22,400	20,900	1.6	60
$PDMS_{137}$–$mPEG_{140}$	1:1.02	82,000			160
$PDMS_{137}$–DMA_{110}/EXA_{66}	1:1.28	30,700			20
$PDMS_{137}$–DMA_{103}/EXA_{25}	1:0.93	24,600			20
$PDMS_{137}$–DMA_{93}/EXA_{14}	1:0.78	22,200			20

[a]A CMC value could not be obtained for Silube as it is not soluble in water [b]Determined using ^{1}H NMR analysis. [c]Determined using SEC analysis. [d]Determined using surface tension analysis.

PDMS (0.975 g/mL), ρ^* is the measured density of individual polyMIPE samples (Table S1), and Φ is the total porosity.

$$\Phi\ (\%) = \left(1 - \frac{\rho^*}{\rho}\right) \times 100 \quad (1)$$

The degree of interconnectivity was calculated using eq 2 where d_p is the average pore diameter and d_{pt} is the average pore throat diameter that was obtained by analysis of SEM images using ImageJ software following protocols from previous reports.[65]

$$\text{Degree of interconnectivity}\ (\%) = \left(\frac{d_{pt}}{d_p}\right) \times 100 \quad (2)$$

Mechanical analysis was performed by using a PerkinElmer dynamic mechanical analyzer (DMA-8000) and processed by using Pyris software. PolyMIPEs were cut into rectangular shapes with dimensions ~3 mm thick, ~6 mm long, and ~3 mm wide. Frequency sweep experiments were performed in rectangular tension mode (0.1–70 Hz; 0.01 mm strain) on three separate samples for all materials and presented as the average of the replicates. The acoustic characterization of samples was performed at ultrasonic frequencies following previously reported protocols.[23,24] For each material, two samples (32 mm in diameter) with different thicknesses (1 and 2 mm) were used. Each sample was placed between two identical broadband ultrasonic (US) transducers (emitter and receiver, Olympus V301) with a diameter of 30 mm and a central frequency of 500 kHz. The US transducers were placed face to face and mounted on a linear manual stage, allowing the precise measurement of the sample thickness, i.e., the propagation distances (d) with an uncertainty of ~100 μm. The emitting transducer was excited with short (broadband) pulses generated by a pulser/receiver (Olympus, 5077PR) that was also used to amplify the electric signal recorded by the receiving transducer before its acquisition on a computer via an oscilloscope.

RESULTS AND DISCUSSION

We prepared ABA triblock copolymer surfactants with a central PDMS-*block* that was chain extended with either DMA, HPMA, mPEG, or a combination of DMA/EXA using RAFT polymerizations with the goal of controlling the morphology (i.e., shape, size, and connectivity on the IP droplets) of the emulsion template (Figure 1). Polymer surfactants containing

https://doi.org/10.1021/acsami.3c14859
ACS Appl. Mater. Interfaces 2023, 15, 58917−58930

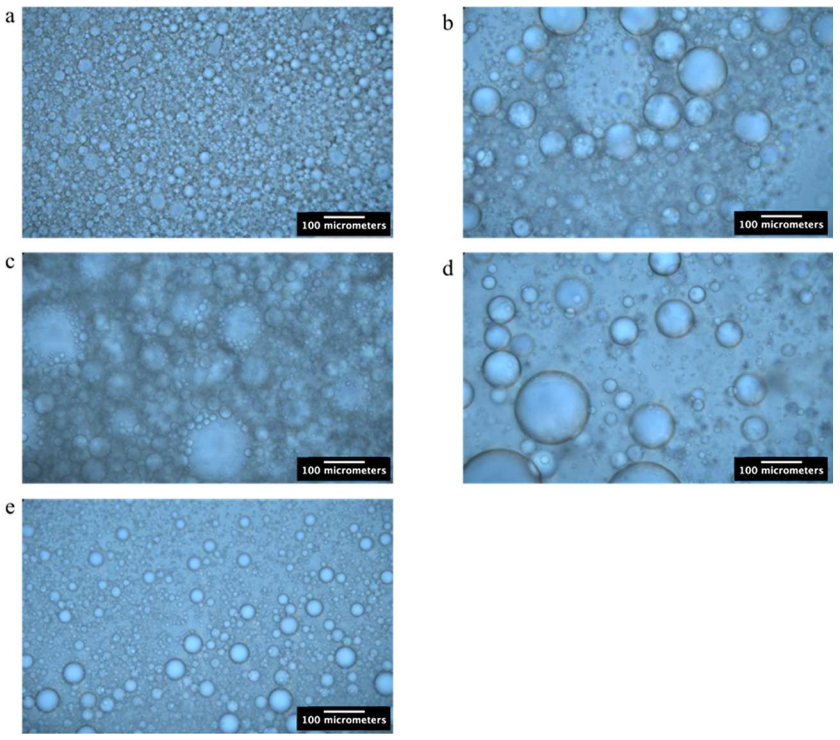

Figure 2. Optical microscopy images of MIPE prepared using various surfactants. (a) Silube, (b) $PDMS_{137}$−DMA_{138}, (c) $PDMS_{137}$−$HPMA_{95}$, (d) $PDMS_{137}$−DMA_{103}/EXA_{25}, and (e) $PDMS_{137}$−$mPEG_{140}$. In each image, the spherical droplets are the aqueous internal phase, and the area surrounding the droplets is the PDMS continuous phase. Scale bar is 100 μm for the image.

poly(DMA-*ran*-EXA) blocks are reactive surfactants, as these surfactants contain pendant-thiol functional groups that can react with the CP of the emulsion during polymerization. The CP used in this work is a combination of thiol- and ene-functionalized PDMSs, and due to the orthogonal nature of thiol−ene "click chemistry", the thiol-containing surfactants can participate in the cross-linking reaction.

These monomers were chosen to impart different chemistry or architectures into the triblock copolymers. Specifically, we selected monomers with different backbone architectures, (i.e., acrylamide and methacrylamide) and monomers that would result in linear or comb polymers. We synthesized surfactants with different hydrophilic block sizes to obtain surfactants with a range of hydrophilicity. We chose these parameters to control the IP droplet size and the IP droplet−droplet interactions in the emulsion templates. We used a PDMS-based macro-CTA synthesized from a commercially available hydroxy-terminated PDMS with a molecular weight of 10,000 g/mol (degree of polymerization ∼137) to prepare all the block copolymer surfactants. The surfactants are named according to the total degree of polymerization of the blocks as determined by NMR analysis. For example, the surfactant $PDMS_{137}$−DMA_{271} has DMA hydrophilic blocks with a degree of polymerization of ∼271 units and an ABA architecture of $poly(DMA)_{136}$-*block*-$poly(dimethylsiloxane)_{137}$-*block*-$poly(DMA)_{136}$. Similarly, $PDMS_{137}$-DMA_{103}/EXA_{25} is a reactive triblock polymer surfactant that has a total hydrophilic block size of ∼128 total units and 25 thiol functional groups within the hydrophilic block, giving a copolymer of $poly[(DMA)_{57}$-*ran*-$(EXA)_{13}]$-*block*-$poly(dimethylsiloxane)_{137}$-*block*-$poly-[(DMA)_{57}$-*ran*-$(EXA)_{13}]$. The surfactants were purified following polymerization by either precipitation or dialysis and characterized by using ^{1}H NMR spectroscopy, SEC, and surface tension measurements, and the results are presented in Table 1.

Surfactants prepared from DMA and HPMA monomers were prepared with theoretical molar block ratios of 1:2, 1:1, and 1:0.5 (PDMS/hydrophilic block), and ^{1}H NMR spectroscopy results of the purified polymers showed good agreement with the expected ratios. The DDMAT CTA end-groups were removed using a postpolymerization radical reaction, as the dodecyl hydrocarbon chains act as hydrophobic groups. Thiol-containing reactive surfactants, $PDMS_{137}$−DMA_x/EXA_y, were prepared with similar total block ratios to the nonreactive surfactants, but with different amounts of thiol functional groups. For these surfactants, we synthesized an acrylate-functionalized xanthate monomer (EXA) following literature protocols[60,61] so as to provide a monomer with a protected thiol that does not act as an additional CTA during the polymerization. We deprotected the thiol using aminolysis with isopropyl amine, which simultaneously removed both the trithiocarbonate from the DDMAT groups and the dithioester of the EXA repeating units to yield free thiols as terminal groups and backbone groups. We confirmed full removal of the thiocarbonyl and ethoxy groups from the polymer by using ^{1}H NMR spectroscopy (Figure S12). Collectively, the observed M_n data obtained using SEC calibrated with polystyrene standards are lower than expected. We attribute this to the poor solubility of the block copolymer surfactants in the mobile phase of the SEC instruments, and this result has also been seen in related reports.[47]

We first prepared water-in-PDMS emulsions that had an IP volume fraction of 60% and the triblock surfactant or Silube was added at 1 wt % (with respect to the weight of CP). The PDMS-based continuous phase consists of a mixture of pendent-thiol- and vinyl-terminated polysiloxanes. We selected

https://doi.org/10.1021/acsami.3c14859
ACS Appl. Mater. Interfaces 2023, 15, 58917−58930

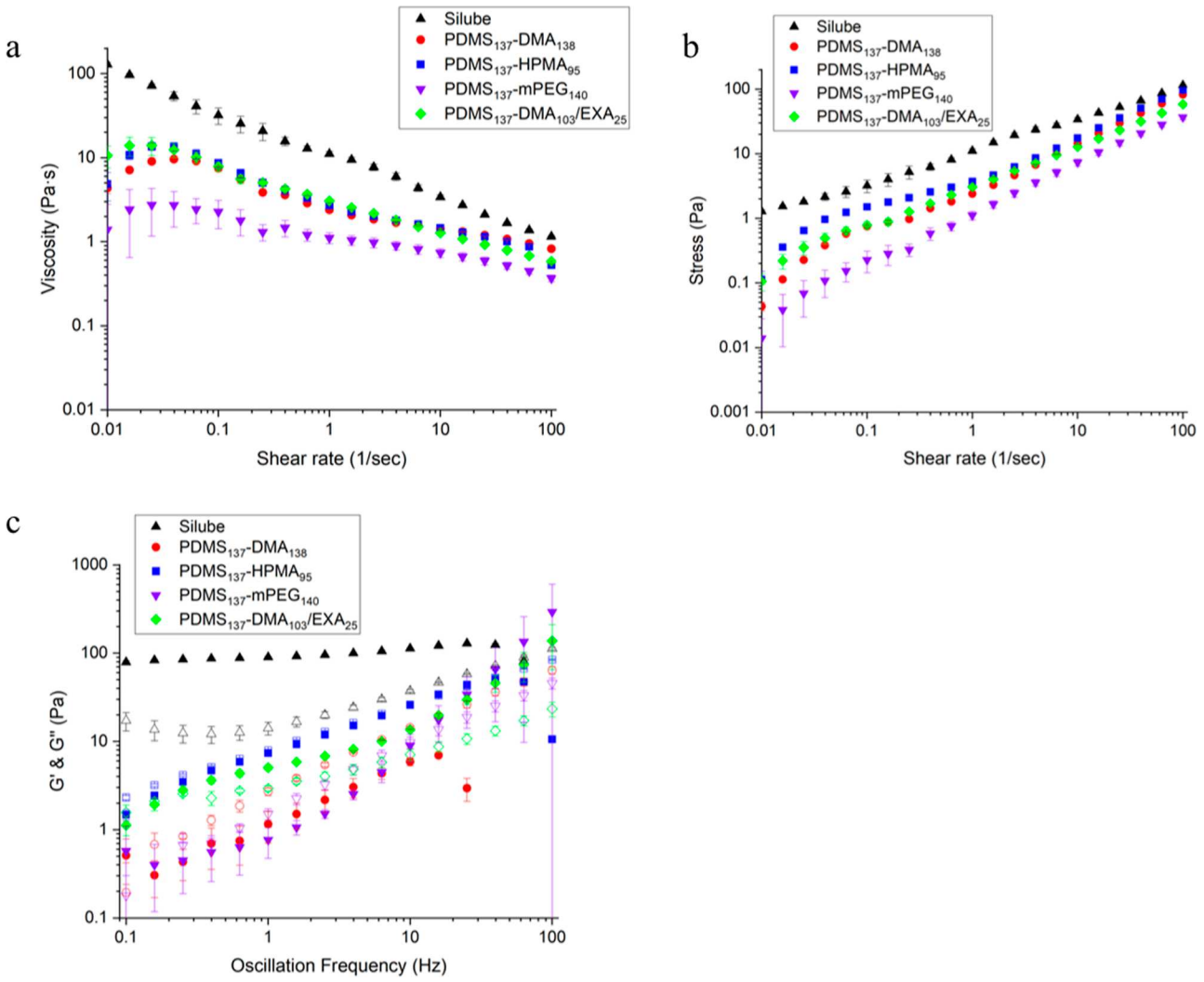

Figure 3. Results of flow sweep (a,b) and frequency sweep (c) rheology experiments on MIPEs stabilized with Silube (black), $PDMS_{137}$−DMA_{138} (red), $PDMS_{137}$−$HPMA_{95}$ (blue), $PDMS_{137}$−$mPEG_{140}$ (purple), and $PDMS_{137}$−DMA_{103}/EXA_{25} (green). Closed symbols are the storage modulus data, and open symbols are the loss modulus data in (c). Data are presented as an average of three replicates for each formulation.

1 wt % for the surfactants as this amount is above the experimentally determined CMC value for each surfactant. We chose to first consider only emulsions at an IP volume fraction of 60% to interrogate the impact of the surfactant on the emulsion properties in a template in which pore collapse was minimized in previous studies. Therefore, any differences in the templates should be captured in the final porous solids. These emulsions are described as MIPEs, as they fall between 25 and 74% IP volume fraction.

MIPEs were characterized by using optical microscopy to obtain the average IP droplet size, shape, and droplet−droplet interactions (i.e., aggregations), and the images are presented in Figure 2. We chose to image emulsions prepared from triblock copolymer surfactants with different A-blocks but equal PDMS block to hydrophilic block ratios.

In these images, MIPE prepared with Silube is presented as a reference (Figure 2a). Silube is a commercially available PDMS-based random brushy copolymer surfactant consisting of a siloxane backbone and pendent PEG chains and is the surfactant we have used in our previous studies.[21,24,27] MIPEs prepared from Silube (Figure 2a) obtained the smallest IP droplets from qualitative analysis of the microscopy images and an aggregated droplet morphology indicated by no observable fully isolated droplets. The IP droplets were more dispersed in size in MIPEs prepared with the block copolymer surfactants than in MIPEs prepared with Silube. For example, MIPEs prepared from $PDMS_{137}$−DMA_{138} had IP droplets that were much larger, ∼100 μm in diameter in some cases, and showed high dispersity in sizes (Figure 2b). The chemistry of the hydrophilic block of the surfactant does not appear to have an effect on the average IP droplet diameter or on the overall qualitative morphology of the emulsion. In contrast to the Silube-stabilized MIPE, MIPEs prepared from the triblock copolymers (Figure 2b−e) possessed IP droplets that do not aggregate and are dispersed through the CP.

MIPEs were characterized using rheology to quantify the differences observed from the microscopy images, and the results of the flow sweep and frequency sweep rheology experiments are presented in Figure 3.

Flow sweep experiments showed that MIPE prepared using Silube obtained the highest viscosity of ∼130 Pa·s at low shear compared to MIPEs prepared using triblock surfactants obtaining viscosities ranging from ∼5−30 Pa·s at low shear (black triangles in Figure 3a). An apparent yield stress of ∼2 Pa is observed for emulsions prepared with Silube, while we observed no apparent yield stress in MIPEs stabilized with the

https://doi.org/10.1021/acsami.3c14859
ACS Appl. Mater. Interfaces 2023, 15, 58917−58930

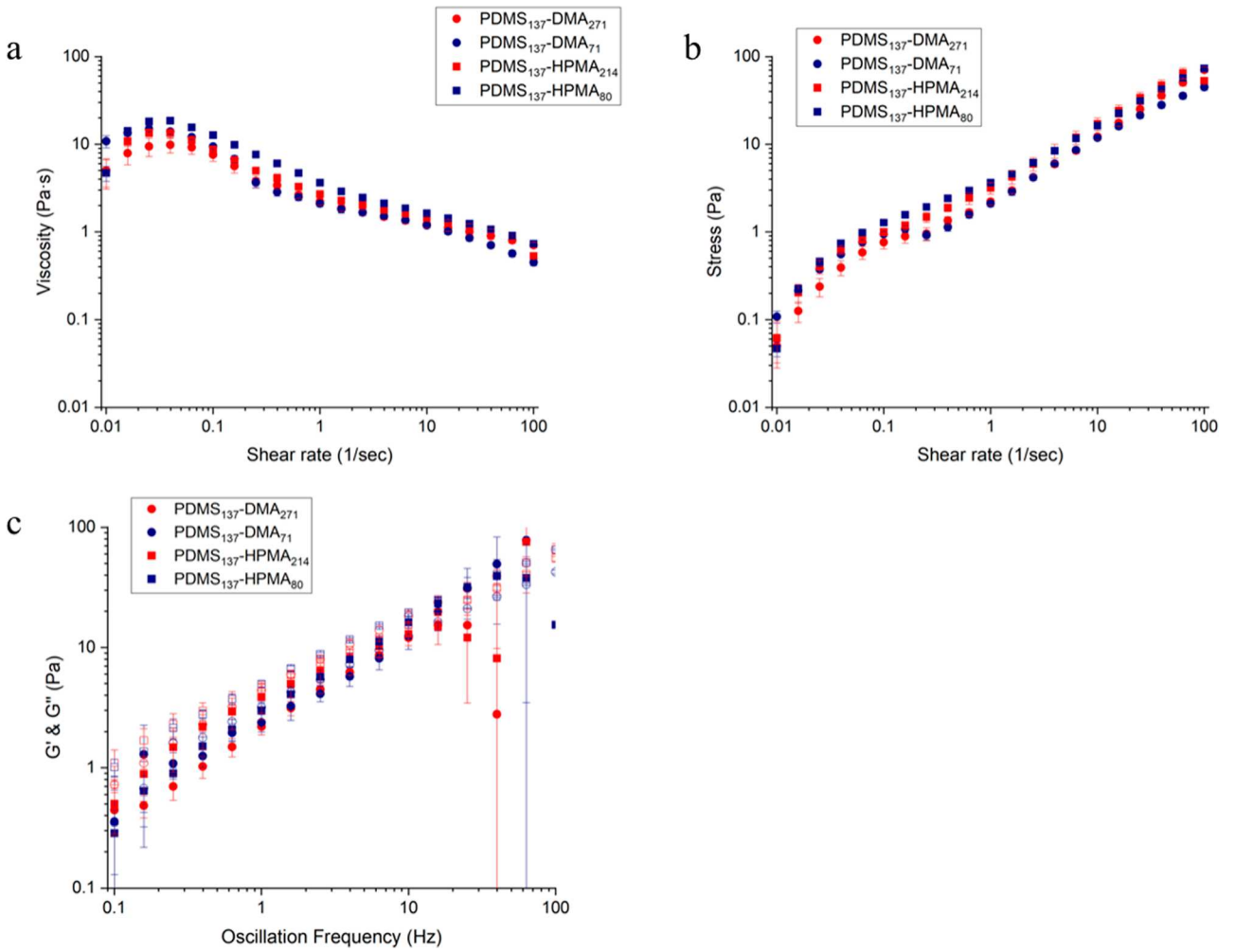

Figure 4. Results of flow sweep (a,b) and frequency sweep (c) rheology experiments on MIPEs stabilized with either PDMS-DMA (circles) or PDMS-HPMA (squares) where the length for the hydrophilic block was of different lengths. Closed symbols are the storage modulus and open symbols are the loss modulus in (c). Data are presented as an average of three replicates for each formulation.

block copolymer surfactants (Figure 3b). Interestingly, the results of the frequency sweep rheology experiments show different properties in the emulsions prepared using Silube compared with the triblock surfactants (Figure 3c). MIPEs prepared from the triblock surfactants display low values of G' and G'' at low frequencies, and the moduli increases with increasing shear rate. MIPEs prepared by using Silube show a different trend in the moduli values obtained during the frequency sweep experiments (open and closed black triangles in Figure 3c). These MIPEs obtain a higher G' than G'' until a crossover point at high shear, and G' remains mostly constant at ∼105 Pa, and this is significantly higher than that of any MIPE prepared by triblock surfactants.

We next prepared emulsions again with an IP volume fraction of 60%, but using triblock surfactants where the length of the poly(DMA) or poly(HPMA) hydrophilic block was varied to probe how this affected emulsion stability and morphology, and the rheology results are presented in Figure 4.

All MIPEs prepared using PDMS-DMA (circles in Figure 4) or PDMS-HPMA (squares in Figure 4) surfactants showed similar viscosities of ∼8−10 Pa·s at low shear and no observable yield stress in the flow sweep rheology experiments. Furthermore, oscillatory frequency sweep experiments (Figure 4c) showed all MIPEs prepared from these surfactants obtained similar G' and G'' values of ∼10 Pa at 10 Hz that increased with shear rate and the G'' was consistently higher than G'. From these rheology experiments, it appears that the length of the hydrophilic block, either larger or smaller than the hydrophobic PDMS block, did not affect the rheological properties of the MIPEs. This result is different than the work of Poling-Skutvik and co-workers[66] where the properties of cyclohexane-in-water emulsions could be changed by the length of the hydrophobic block of poly(ethylene oxide)/polystyrene (PEO/PS) ABA triblock copolymer surfactants. In that work, emulsions prepared using triblock copolymer surfactants with the largest terminal PS blocks obtained G' values of ∼180 Pa compared to ∼10 Pa for emulsions prepared from surfactants with the lowest PS content due to the ability of surfactants with larger PS blocks to "bridge" different nanosized cyclohexane droplets causing an increase in the elasticity of the emulsion. We propose that this difference in our work is due to the difference in the size of the emulsion droplets. The emulsion droplets stabilized with triblock copolymer surfactants in our work are much larger (∼100×) than those of Poling-Skutvik and co-workers and likely too large to undergo any surfactant bridging.[67]

https://doi.org/10.1021/acsami.3c14859
ACS Appl. Mater. Interfaces 2023, 15, 58917−58930

Scheme 1. Cartoon Reaction Scheme Detailing the Thiol−Ene Crosslinking Reaction Occurring in the CP to Prepare PolyMIPEs

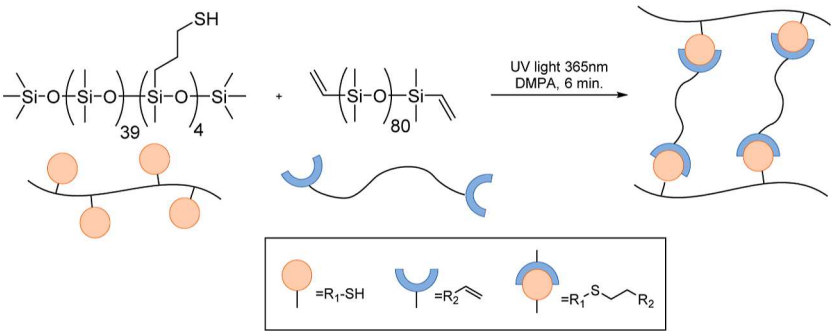

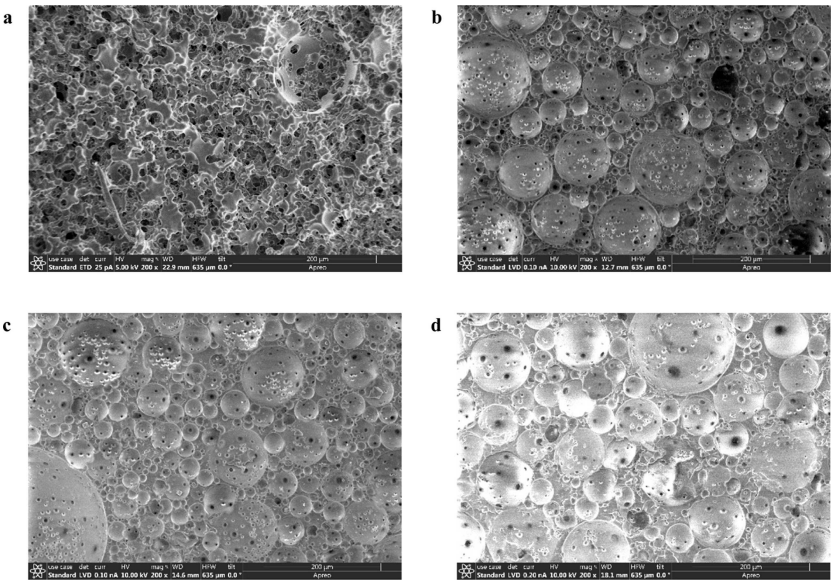

Figure 5. SEM images of polyMIPEs prepared from (a) Silube, (b) $PDMS_{137}$−DMA_{138}, (c) $PDMS_{137}$−$HPMA_{95}$, or (d) $PDMS_{137}$−DMA_{103}/EXA_{25} as the surfactant. The scale bar is 200 μm in each image.

Table 2. Total Porosity Results, Average Pore Diameter (d_p), Average Pore Throat Diameter (d_{pt}), and Degree of Interconnectivity of polyMIPEs Prepared with the Various Surfactants

surfactant	Φ_{theo} [a] (%)	Φ_{exp} [b] (%)	d_p [c] (μm)	d_{pt} [c] (μm)	degree of interconnectivity [d] (%)
silube	60	58 ± 1	16 ± 6	6 ± 2	40
	70	62 ± 2	11 ± 5	6 ± 2	55
	75	53 ± 2			
$PDMS_{137}$−DMA_{138}	60	54 ± 1	40 ± 20	4 ± 1	10
	70	67 ± 2	32 ± 18	3 ± 1	11
	75	71 ± 2	36 ± 25	5 ± 2	13
$PDMS_{137}$−$HPMA_{95}$	60	55 ± 1	36 ± 22	4 ± 2	12
	70	67 ± 2	37 ± 23	4 ± 1	11
	75	71 ± 2	31 ± 16	4 ± 2	14
$PDMS_{137}$−DMA_{110}/EXA_{66}	60	56 ± 1	36 ± 21	5 ± 2	14
	70	65 ± 2	35 ± 20	4 ± 2	12
	75	69 ± 2	30 ± 18	4 ± 2	14
$PDMS_{137}$−DMA_{103}/EXA_{25}	60	57 ± 1	32 ± 20	4 ± 2	14
	70	66 ± 2	34 ± 22	4 ± 2	12
	75	71 ± 2	32 ± 20	5 ± 2	15
$PDMS_{137}$−DMA_{93}/EXA_{14}	60	54 ± 1	37 ± 21	5 ± 2	14
	70	64 ± 2	36 ± 20	4 ± 2	12
	75	71 ± 2	30 ± 18	4 ± 2	14

[a]Initial internal phase volume fraction in the emulsion. [b]Calculated from eq 1. [c]Measured from 100 pores or pore throats from 2 SEM images of replicate materials. [d]Calculated from eq 2.

https://doi.org/10.1021/acsami.3c14859
ACS Appl. Mater. Interfaces 2023, 15, 58917−58930

We next prepared emulsions with IP volume fractions of 70 and 75% to examine whether the triblock surfactants could produce stable templates for higher porosity materials. Each surfactant was able to prepare stable emulsions up to 75% except $PDMS_{137}$−DMA_{71} and $PDMS_{137}$−$mPEG_{140}$. Emulsions prepared by using $PDMS_{137}$−DMA_{71} and $PDMS_{137}$−$mPEG_{140}$ experienced phase inversion to PDMS-in-water emulsions at IP volume fractions over 70%. Phase inversion has been shown to occur in emulsions stabilized with block copolymer surfactants with an asymmetric hydrophilic to hydrophobic ratio as the volume fraction of the IP is changed.[68] Based on this result, we chose to prepare only emulsion-templated polymers using emulsions that did not experience phase inversion over the full range of IP volume fractions examined.

We synthesized emulsion-templated polymer materials by preparing emulsions with a photoinitiator (DMPA) dissolved in the continuous phase to initiate the thiol−ene cross-linking occurring between thiolated-PDMS and vinyl-terminated PDMS (Scheme 1).

The polyMIPEs were prepared with an equal thiol−ene molar ratio in the continuous phase, 1 wt % photoinitiator, and using 1 wt % of the triblock surfactants or Silube in emulsions with an IP volume fraction of 60, 70, or 75%. The CP of the emulsions was polymerized, dried, and characterized using SEM imaging, and the images of cross sections from dried polyMIPEs prepared from emulsions with an IP volume fraction of 75% are presented in Figure 5. These images are representative of the remaining formulations, and the SEM images of 60 and 70% porosity polyMIPEs are presented in Figure S14.

PolyMIPEs prepared by using Silube as the surfactant (Figure 5a) show a morphology consisting of aggregated pores and a loss of a distinct spherical pore structure, consistent with our previous publications. In contrast, the polyMIPEs prepared using the triblock copolymer surfactants (Figure 5b−d) have similar isolated and open pore morphologies with small pore throats between pores that are noticeably different from the morphology observed for polyMIPEs prepared using Silube. Distinct spherical pores are observed that are surrounded by a polymer wall, and the pores have a dispersity in size. Importantly, there does not appear to be appreciable pore collapse for these polyMIPEs from a comparison of the calculated total porosity calculations (Φ_{exp}) and theoretical values, as shown in Table 2.

PolyMIPEs prepared using $PDMS_{137}$−DMA_{138} in the emulsion template obtained porosities as high as 71%, and we observed Φ_{exp} values that are only ∼5% lower than the theoretical values. In contrast, polyMIPEs prepared from Silube show significant pore collapse at porosities over 60% with Φ_{exp} ∼20% lower than the expected theoretical value due to pore collapse when an emulsion template with 75% IP volume fraction was used. Similar pore collapse has been observed in our previous work[27,35] and work from others[34] with soft, porous materials made from polymers with low glass-transition temperatures. The observed pore collapse is typically caused by capillary forces experienced during the drying process as the internal phase is removed from the porous material. We hypothesize that the reduction in pore collapse observed from emulsion templates prepared with the triblock copolymer surfactants is due to the differences that were observed in the microscopy and rheology results, and these differences are also displayed in the pore structure for polyMIPEs prepared using these surfactants. The polyMIPEs prepared using Silube possessed the smallest d_p (∼15 μm) and d_{pt} (∼6 μm) for polyMIPEs having a porosity of ∼50−60%. The polyMIPEs prepared using the triblock surfactants have similar d_p and d_{pt} values of ∼35 and ∼3 μm, respectively, indicating that these materials had pores that were larger on average with smaller pore throats than polyMIPEs prepared using Silube. PolyMIPEs prepared using Silube possessed the highest degree of interconnectivity. The polyMIPEs prepared using triblock copolymer surfactants obtain much lower interconnectivity values, even for polyMIPEs having an Φ_{exp} higher than 70%. The differences in interconnectivity are again explained through the differences in the emulsion templates where the differences observed in the microscopy images of the emulsions are observed in the polymerized materials, and a more isolated pore morphology is observed in materials where the IP droplets were isolated in the MIPE or HIPE template.

We hypothesized that the polyMIPEs prepared here would have different mechanical properties due to the large morphological differences seen in the SEM imaging, resulting from the surfactant chosen to prepare the emulsion. To test this, we performed dynamic mechanical analysis on the polyMIPEs, and the results are presented in Figure 6. The storage modulus (G') remained constant over the frequency range tested, and the average G' for each material is reported at 10 Hz for different Φ_{exp} values for simplicity.

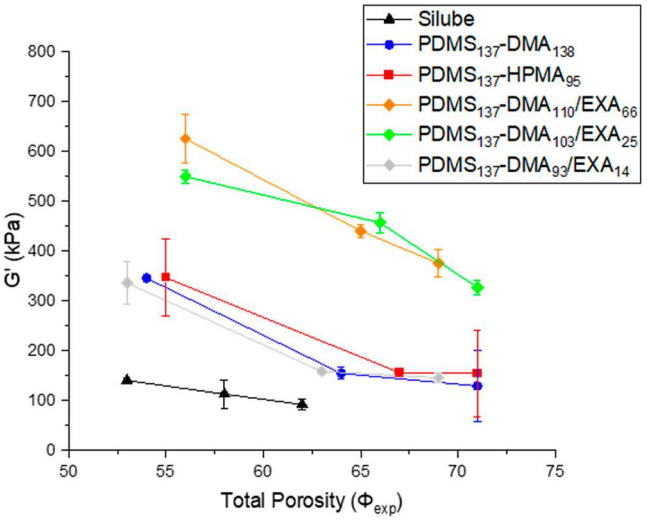

Figure 6. Storage modulus versus experimental total porosity for polyMIPEs prepared using Silube (black), $PDMS_{137}$−DMA_{138} (blue), $PDMS_{137}$−$HPMA_{95}$ (red), $PDMS_{137}$−DMA_{110}/EXA_{66} (orange), $PDMS_{137}$−DMA_{103}/EXA_{25} (green), and $PDMS_{137}$−DMA_{93}/EXA_{14} (gray). The dashed lines are to guide the eye. Each data point is the average of three replicates.

As expected, we observed an inverse relationship between the G' and Φ_{exp} for the polyMIPEs for all the surfactants examined. Significantly, we observed a marked difference in the G' of the polyMIPEs prepared using reactive surfactants compared to the nonreactive triblock copolymer surfactants. Specifically, polyMIPEs prepared using $PDMS_{137}$−DMA_{110}/EXA_{66} and $PDMS_{137}$−DMA_{103}/EXA_{25} reactive block copolymer surfactants had the highest G' values over the entire Φ_{exp} range examined in this work. For example, $PDMS_{137}$−DMA_{110}/EXA_{66} and $PDMS_{137}$−DMA_{103}/EXA_{25} had similar G' values of ∼460−360 kPa at Φ_{exp} of ∼65−70% (orange and green diamonds in Figure 6, respectively). In contrast,

https://doi.org/10.1021/acsami.3c14859
ACS Appl. Mater. Interfaces 2023, 15, 58917−58930

polyMIPEs prepared using the nonreactive surfactants $PDMS_{137}$–DMA_{138} (blue circles in Figure 6) and $PDMS_{137}$–$HPMA_{95}$ (red squares in Figure 6) had a lower value of G' of ~180 kPa for a similar Φ_{exp} range than was seen for the reactive surfactants. We hypothesize that the increase in G' is due to a strengthening of the pore walls due to the reactive surfactant participating in the thiol–ene reactions localized at the pore wall occurring during the CP during polymerization. Recent work by Bismarck, Jiang, and co-workers[46] also showed that using polymeric surfactants resulted in an increase in compressive moduli compared to small molecule surfactants, and they attributed this to the polymeric surfactant strengthening the pore wall struts by becoming entangled within the polymer network, rather than cross-linked into the network as is the case in our work. Debuigne and co-workers[53] also reported that covalently bonding CTA-terminated RAFT surfactants to the walls of a polyHIPE resulted in polyHIPEs with higher mechanical properties due to differences in the interconnectivity of the pores compared to polyHIPEs using surfactants that were physically anchored or not anchored at all. In contrast, in our work, we do not observe any significant changes in pore morphology between reactive and nonreactive surfactants, and therefore we believe this is the first example, to our knowledge, where differences in mechanical properties are due to reinforcing the pore wall by covalent incorporation of the surfactant. Interestingly, the polyMIPE prepared using the reactive surfactant with the lowest thiol-functionality, $PDMS_{137}$–DMA_{93}/EXA_{14}, had G' values of ~200 kPa at ~60 and 70% Φ_{exp} and was similar to the nonthiol-containing surfactants. From this result, it appears that there is a minimal number of pendent thiols, and subsequently minimum cross-linking of the surfactant into the polyMIPE network, required to see any increase in the storage modulus of the resulting polyMIPEs. We hypothesize that this may be due to some thiol-groups not participating in cross-linking with the divinyl PDMS in the CP. This could happen for all the thiol-containing surfactants, but the surfactants with the lowest number of thiols do not participate in cross-linking to a sufficient extent to positively impact the storage modulus of the polyMIPE. The type of backbone functionality of the hydrophilic block in the surfactants, either acrylamide or methacrylate, did not have an impact on the G' of the polyMIPEs produced. Moreover, the length of the hydrophilic block in the surfactant used to prepare the materials did not impact the G' of the polyMIPEs, and the polyMIPEs prepared using surfactants synthesized with either DMA or HPMA as the hydrophilic block all obtained similar G' values (Figure S15).

The G' observed in $PDMS_{137}$–DMA_{138} and $PDMS_{137}$–$HPMA_{95}$ was higher than that seen in polyMIPEs prepared using Silube, even at the lower Φ_{exp} values obtained in the polyMIPEs prepared using Silube before pore collapse occurred. The polyMIPEs prepared using Silube possessed the lowest G' of all the materials prepared in this work with values of ~100 kPa at a Φ_{exp} of ~60% (black triangles in Figure 6). This result is explained due to the morphology of these materials, as polyHIPEs that have small and highly interconnected pores are typically weaker than similar polyHIPEs that have larger or less interconnected pores (i.e., closed-cell morphologies).[38,39] Collectively, the mechanical analysis of these polyMIPEs shows that G' can be changed solely by the architecture and chemistry of the surfactant. This result is significant as there have been limited reports of reactive surfactants used to control material properties without impacting the pore morphology. We believe that this result could be translated to other block copolymer-stabilized emulsion-templated materials to further expand the capabilities of polymer surfactants in the field of polyHIPEs.

Considering that the polyMIPEs prepared using the reactive and nonreactive triblock surfactants possessed higher storage moduli and higher porosities than those prepared in our previous publications,[23,24] we anticipated that these materials may have different acoustic properties than our previous materials. This is because both the storage moduli and the porosity of soft, porous PDMS materials have been demonstrated to modulate the longitudinal speed of sound (C_L) moving through them.[18,20] The control of C_L is a key feature leading to these materials being proposed as candidates for use in metasurfaces, lenses, and other acoustic devices.[19,20] Therefore, the acoustic properties of the polyMIPEs prepared using triblock surfactants were tested at ultrasonic frequencies, and the results are presented in Figure 7.

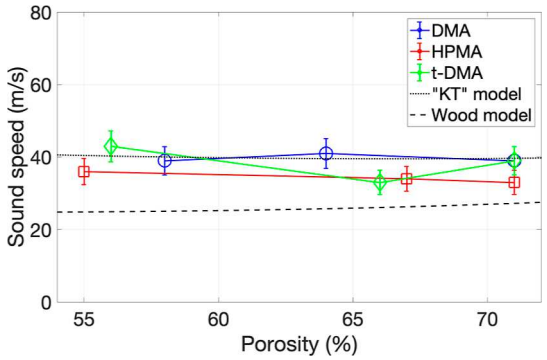

Figure 7. Sound speed versus porosity for polyMIPEss prepared by using $PDMS_{137}$–DMA_{138} (blue), $PDMS_{137}$–$HPMA_{95}$ (red), and $PDMS_{137}$–DMA_{103}/EXA_{25} (green) as the surfactant. The dashed lines are representative of the Kuster–Toksöz (thin dotted line) and Wood (thick dashed line) mathematical models. The solid-colored lines are used to guide the eye.

We observed particularly low longitudinal sound speeds (C_L) of ~30–40 m/s for all the polyMIPEs tested in this work at ultrasonic frequencies regardless of differences in the storage moduli of the materials at higher porosities. These results expand on our previous work[23,24] where PDMS polyMIPEs prepared with a much lower Φ_{exp} of 40% using Silube resulted in C_L values of ~50 m/s. In the work presented here, we have been able to obtain soft PDMS polyMIPEs by using triblock surfactants, and these polyMIPEs have Φ_{exp} values greater than those previously unobtainable when using Silube as the surfactant. The materials prepared in this work all obtain C_L values of ~35 m/s independent of porosity or morphology and these values are closely similar to predictions from both the Wood model[69] usually used for bubbly liquids (thick dashed line in Figure 7) and the Kuster–Toksöz model[70] derived for solid composite media (thin dashed line in Figure 7). Both models have been already used successfully to calculate the effective sound speed of porous materials that have low G' values.[18] Interestingly, the values of C_L observed over these materials and our previously reported polyMIPEs[23] do not appear to be greatly affected by the total porosity of the material or the morphology of the polyMIPEs, and they follow the wide plateau of C_L with changing porosity expected in

https://doi.org/10.1021/acsami.3c14859
ACS Appl. Mater. Interfaces 2023, 15, 58917–58930

materials with porosities over 30% seen in the Kuster−Toksöz model. Importantly, the materials prepared in this work provide further experimental validation of these models in porous PDMS at higher porosity values than those previously reported. We envision these polyMIPEs to be good candidates for the preparation of acoustic devices or acoustic metasurfaces that can obtain low sound speeds in the ultrasonic frequency range.

CONCLUSIONS

We have used reactive block copolymer surfactants to control the porosity and morphology of soft PDMS-based polyMIPEs, allowing us to test the acoustic properties of these materials at higher porosities than previously achievable. Interestingly, we have found that the longitudinal sound speed observed through these materials is similar to that observed in materials with porosities of around 40 and 60%. This would imply that total porosity only affects the sound speed in these very soft materials at porosities below ∼30% based on reports from Brunet and Mondain-Monval. It remains an open question if very high porosities (e.g., >85%) would also modulate observed values of C_L. It appears that the acoustic properties of these materials are dominated by their low storage moduli, and future studies are required to probe how sound speeds may be modulated by materials of different moduli at a single porosity, where the materials presented here will likely represent the lower bound in achievable sound speeds. Significantly in this work, polyMIPEs prepared from block copolymer surfactants showed minimal pore collapse and could obtain Φ_{exp} values of up to 71% under standard drying conditions. Furthermore, polyMIPEs prepared from thiol-containing reactive surfactants obtained the values of ∼350 kPa at a Φ_{exp} of ∼70% compared to nonreactive surfactants that obtained a G' value of ∼180 kPa at a similar Φ_{exp}. Importantly, these differences in moduli were dependent on the functionality of the surfactant, and the porosity and pore morphology of the polyMIPE were unaffected by the choice of reactive or nonreactive surfactant. We expect that this result can be translated to other fields of emulsion-templated materials such as tissue engineering scaffolds and separation membranes where there is a need for controlling the stiffness of the material without impacting pore size or interconnectivity. Collectively, our findings suggest that these materials are good candidates for use in acoustic materials, including ultrasonic frequency wave dampening and waveguiding devices.

ASSOCIATED CONTENT

Supporting Information

The Supporting Information is available free of charge at https://pubs.acs.org/doi/10.1021/acsami.3c14859.

Additional information such as ^{1}H and ^{13}C NMR spectroscopy of compounds and surfactants, digital images of surfactants after end-group removal or deprotection reactions, density measurements of polyMIPEs, SEM images of polyMIPEs prepared from the different surfactants at 60 and 70% theoretical porosity, and DMA results from polyMIPEs prepared from either PDMS−DMA or PDMS−HPMA surfactants with different hydrophilic block sizes (PDF)

AUTHOR INFORMATION

Corresponding Author

Neil Ayres − *Department of Chemistry, The University of Cincinnati, Cincinnati, Ohio 45221, United States;* orcid.org/0000-0001-8718-2502; Email: neil.ayres@uc.edu

Authors

Tucker J. McKenzie − *Department of Chemistry, The University of Cincinnati, Cincinnati, Ohio 45221, United States*

Thomas Brunet − *Institut de Mécanique et d'Ingénierie, University of Bordeaux—CNRS—Bordeaux INP, Talence 33405, France*

Lyndsay N. Kissell − *Department of Chemistry, University of Cincinnati, Cincinnati, Ohio 45221, United States*

Pietro Strobbia − *Department of Chemistry, University of Cincinnati, Cincinnati, Ohio 45221, United States;* orcid.org/0000-0003-0884-6185

Complete contact information is available at: https://pubs.acs.org/10.1021/acsami.3c14859

Author Contributions

The manuscript was written through contributions of all authors. All authors have given approval to the final version of the manuscript.

Notes

The authors declare no competing financial interest.

ACKNOWLEDGMENTS

T.J.M and N.A. thank the National Science Foundation (DMR-1940518) for the resources to conduct this work, Dr. Spencer Hendrickson and Prof. Ryan White for help with 3D printing of the templates used in this work, and Dr. Melodie Fickenscher for help with obtaining the SEM images.

REFERENCES

(1) Li, Y.; Ji, N.; Qu, H.; Lin, J.; Wang, D.; Meng, R.; Li, B.; Wang, L.; Li, S. Viscoelastic Polyacrylate with Hierarchical Hollow Zeolite for Sound Insulation. *J. Appl. Polym. Sci.* **2023**, *140* (25), 53976.

(2) Chen, H.; Li, X. P.; Chen, Y. Y.; Huang, G. L. Wave Propagation and Absorption of Sandwich Beams Containing Interior Dissipative Multi-Resonators. *Ultrasonics* **2017**, *76*, 99−108.

(3) Babaee, S.; Overvelde, J. T. B.; Chen, E. R.; Tournat, V.; Bertoldi, K. Reconfigurable Origami-Inspired Acoustic Waveguides. *Sci. Adv.* **2016**, *2* (11), 1601019.

(4) Guillermic, R. M.; Lanoy, M.; Strybulevych, A.; Page, J. H. A PDMS-Based Broadband Acoustic Impedance Matched Material for Underwater Applications. *Ultrasonics* **2019**, *94*, 152−157.

(5) Cai, Z.; Zhao, S.; Huang, Z.; Li, Z.; Su, M.; Zhang, Z.; Zhao, Z.; Hu, X.; Wang, Y. S.; Song, Y. Bubble Architectures for Locally Resonant Acoustic Metamaterials. *Adv. Funct. Mater.* **2019**, *29* (51), 1906984.

(6) Popa, B.-I.; Wang, W.; Konneker, A.; Cummer, S. A.; Rohde, C. A.; Martin, T. P.; Orris, G. J.; Guild, M. D. Anisotropic Acoustic Metafluid for Underwater Operation. *J. Acoust. Soc. Am.* **2016**, *139* (6), 3325−3331.

(7) Wen, J.; Zhao, H.; Lv, L.; Yuan, B.; Wang, G.; Wen, X. Effects of Locally Resonant Modes on Underwater Sound Absorption in Viscoelastic Materials. *J. Acoust. Soc. Am.* **2011**, *130* (3), 1201−1208.

(8) Jin, Y.; Zhou, M.; Choi, T. Y.; Neogi, A. Thermally Tunable Acoustic Beam Splitter Based on Poly(Vinyl Alcohol) Poly(n-Isopropylacrylamide) Hydrogel. *Gels* **2021**, *7* (3), 140.

(9) Hussein, M. I.; Frazier, M. J. Metadamping: An Emergent Phenomenon in Dissipative Metamaterials. *J. Sound Vib.* **2013**, *332* (20), 4767−4774.
(10) Cummer, S. A.; Christensen, J.; Alù, A. Controlling Sound with Acoustic Metamaterials. *Nat. Rev. Mater.* **2016**, *1*, 16001.
(11) Liu, Z.; Zhang, X.; Mao, Y.; Zhu, Y. Y.; Yang, Z.; Chan, C. T.; Sheng, P. Locally Resonant Sonic Materials. *Science* **2000**, *289* (5485), 1734−1736.
(12) Li, Y.; Wang, S.; Peng, Q.; Zhou, Z.; Yang, Z.; He, X.; Li, Y. Active Control of Graphene-Based Membrane-Type Acoustic Metamaterials Using a Low Voltage. *Nanoscale* **2019**, *11* (35), 16384−16392.
(13) Deng, H.; Xu, X.; Zhang, C.; Su, J. W.; Huang, G.; Lin, J. Deterministic Self-Morphing of Soft-Stiff Hybridized Polymeric Films for Acoustic Metamaterials. *ACS Appl. Mater. Interfaces* **2020**, *12* (11), 13378−13385.
(14) Guild, M. D.; García-Chocano, V. M.; Sánchez-Dehesa, J.; Martin, T. P.; Calvo, D. C.; Orris, G. J. On the Use of Aerogel as a Soft Acoustic Metamaterial for Airborne Sound. *Phys. Rev. Appl.* **2015**, *5* (3), 034012.
(15) Zhao, H.; Liu, Y.; Wen, J.; Yu, D.; Wen, X. Dynamics and Sound Attenuation in Viscoelastic Polymer Containing Hollow Glass Microspheres. *J. Appl. Phys.* **2007**, *101* (12), 123518.
(16) Baird, A. M.; Kerr, F. H.; Townend, D. J. Wave Propagation in a Viscoelastic Medium Containing Fluid-Filled Microspheres. *J. Acoust. Soc. Am.* **1999**, *105* (3), 1527−1538.
(17) Ba, A.; Kovalenko, A.; Aristégui, C.; Mondain-Monval, O.; Brunet, T. Soft Porous Silicone Rubbers with Ultra-Low Sound Speeds in Acoustic Metamaterials. *Sci. Rep.* **2017**, *7* (1), 40106.
(18) Kovalenko, A.; Fauquignon, M.; Brunet, T.; Mondain-Monval, O. Tuning the Sound Speed in Macroporous Polymers with a Hard or Soft Matrix. *Soft Matter* **2017**, *13* (25), 4526−4532.
(19) Lombard, O.; Kumar, R.; Mondain-Monval, O.; Brunet, T.; Poncelet, O. Quasi-Flat High-Index Acoustic Lens for 3D Underwater Ultrasound Focusing. *Appl. Phys. Lett.* **2022**, *120* (22), 221701.
(20) Jin, Y.; Kumar, R.; Poncelet, O.; Mondain-Monval, O.; Brunet, T. Flat Acoustics with Soft Gradient-Index Metasurfaces. *Nat. Commun.* **2019**, *10* (1), 143.
(21) Kovalenko, A.; Zimny, K.; Mascaro, B.; Brunet, T.; Mondain-Monval, O. Tailoring of the Porous Structure of Soft Emulsion-Templated Polymer Materials. *Soft Matter* **2016**, *12* (23), 5154−5163.
(22) Zimny, K.; Merlin, A.; Ba, A.; Aristégui, C.; Brunet, T.; Mondain-Monval, O. Soft Porous Silicone Rubbers as Key Elements for the Realization of Acoustic Metamaterials. *Langmuir* **2015**, *31* (10), 3215−3221.
(23) McKenzie, T. J.; Rost, K.; Smail, S.; Mondain-Monval, O.; Brunet, T.; Ayres, N. Mechanically Tunable PDMS-Based PolyHIPE Acoustic Materials. *J. Mater. Chem. C* **2022**, *10* (16), 6222−6226.
(24) McKenzie, T. J.; Heaton, P. S.; Rishi, K.; Kumar, R.; Brunet, T.; Beaucage, G.; Mondain-Monval, O.; Ayres, N. Storage Moduli and Porosity of Soft PDMS PolyMIPEs Can Be Controlled Independently Using Thiol-Ene Click Chemistry. *Macromolecules* **2020**, *53* (10), 3719−3727.
(25) Kumar, R.; Jin, Y.; Marre, S.; Poncelet, O.; Brunet, T.; Leng, J.; Mondain-Monval, O. Drying Kinetics and Acoustic Properties of Soft Porous Polymer Materials. *J. Porous Mater.* **2021**, *28* (1), 249−259.
(26) Pragya, A.; Ghosh, T. K. Soft Functionally Gradient Materials and Structures - Natural and Manmade: A Review. *Adv. Mater.* **2023**, *35* (47), 2300912.
(27) McKenzie, T. J.; Smail, S.; Rost, K.; Rishi, K.; Beaucage, G.; Ayres, N. Multi-Layered Polymerized High Internal Phase Emulsions with Controllable Porosity and Strong Interfaces. *Polymer* **2021**, *231*, 124116.
(28) Smith, A.; Ayres, N. Open-Cell PDMS PolyHIPEs Prepared Using Polymethylvinylsiloxane to Prevent Pore Collapse. *Polymer* **2023**, *270*, 125787.
(29) Grosse, M.-T.; Lamotte, M.; Birot, M.; Deleuze, H. Preparation of Microcellular Polysiloxane Monoliths. *J. Polym. Sci., Part A: Polym. Chem.* **2008**, *46* (1), 21−32.
(30) Ungureanu, S.; Birot, M.; Laurent, G.; Deleuze, H.; Babot, O.; Julián-López, B.; Achard, M. F.; Popa, M. I.; Sanchez, C.; Backov, R. One-Pot Syntheses of the First Series of Emulsion Based Hierarchical Hybrid Organic-Inorganic Open-Cell Monoliths Possessing Tunable Functionality (Organo-Si(HIPE) Series). *Chem. Mater.* **2007**, *19* (23), 5786−5796.
(31) Aldemir Dikici, B.; Claeyssens, F. Basic Principles of Emulsion Templating and Its Use as an Emerging Manufacturing Method of Tissue Engineering Scaffolds. *Front. Bioeng. Biotechnol.* **2020**, *8*, 875.
(32) Stubenrauch, C.; Menner, A.; Bismarck, A.; Drenckhan, W. Emulsion and Foam Templating—Promising Routes to Tailor-Made Porous Polymers. *Angew. Chem., Int. Ed.* **2018**, *57* (32), 10024−10032.
(33) Cameron, N. R. High Internal Phase Emulsion Templating as a Route to Well-Defined Porous Polymers. *Polymer* **2005**, *46* (5), 1439−1449.
(34) Diego, R. B.; Ribelles, J. L. G.; Sánchez, M. S. Pore Collapse during the Fabrication Process of Rubber-like Polymer Scaffolds. *J. Appl. Polym. Sci.* **2007**, *104* (3), 1475−1481.
(35) McKenzie, T. J.; Cawood, C.; Davis, C.; Ayres, N. Synthesis of Patterned PolyHIPE-Hydrogel Composite Materials Using Thiol-Ene Chemistry. *J. Colloid Interface Sci.* **2023**, *645*, 502−512.
(36) Aldemir Dikici, B.; Sherborne, C.; Reilly, G. C.; Claeyssens, F. Emulsion Templated Scaffolds Manufactured from Photocurable Polycaprolactone. *Polymer* **2019**, *175*, 243−254.
(37) Karageorgiou, V.; Kaplan, D. Porosity of 3D Biomaterial Scaffolds and Osteogenesis. *Biomaterials* **2005**, *26* (27), 5474−5491.
(38) Huš, S.; Krajnc, P. PolyHIPEs from Methyl Methacrylate: Hierarchically Structured Microcellular Polymers with Exceptional Mechanical Properties. *Polymer* **2014**, *55* (17), 4420−4424.
(39) Li, K.; Gao, X. L.; Subhash, G. Effects of Cell Shape and Strut Cross-Sectional Area Variations on the Elastic Properties of Three-Dimensional Open-Cell Foams. *J. Mech. Phys. Solids* **2006**, *54* (4), 783−806.
(40) Wong, L. L. C.; Baiz Villafranca, P. M.; Menner, A.; Bismarck, A. Hierarchical Polymerized High Internal Phase Emulsions Synthesized from Surfactant-Stabilized Emulsion Templates. *Langmuir* **2013**, *29* (20), 5952−5961.
(41) Foudazi, R. HIPEs to PolyHIPEs. *React. Funct. Polym.* **2021**, *164* (April), 104917.
(42) Quell, A.; De Bergolis, B.; Drenckhan, W.; Stubenrauch, C. How the Locus of Initiation Influences the Morphology and the Pore Connectivity of a Monodisperse Polymer Foam. *Macromolecules* **2016**, *49* (14), 5059−5067.
(43) Dabrowski, M. L.; Jenkins, D.; Cosgriff-Hernandez, E.; Stubenrauch, C. Methacrylate-Based Polymer Foams with Controllable Connectivity, Pore Shape, Pore Size and Polydispersity. *Phys. Chem. Chem. Phys.* **2020**, *22* (1), 155−168.
(44) Silverstein, M. S. Emulsion-Templated Polymers: Contemporary Contemplations. *Polymer* **2017**, *126* (22), 261−282.
(45) Dhavalikar, P.; Shenoi, J.; Salhadar, K.; Chwatko, M.; Rodriguez-Rivera, G.; Cheshire, J.; Foudazi, R.; Cosgriff-Hernandez, E. Engineering Toolbox for Systematic Design of Polyhipe Architecture. *Polymers* **2021**, *13* (9), 1479.
(46) Muratspahić, E.; Schöffmann, J.; Jiang, Q.; Bismarck, A. Poly(Acrylamide-Co-Styrene): A Macrosurfactant for Oil/Water Emulsion Templating toward Robust Macroporous Hydrogels. *Macromolecules* **2023**, *56* (8), 3213−3223.
(47) Li, J. J.; Wu, Y.; Luo, Z. H.; Zhou, Y. N. Hydrophilic Macroporous Monoliths with Tunable Water Uptake Capacity Fabricated by Water-in-Oil High Internal Phase Emulsion Templating. *J. Polym. Sci.* **2022**, *60* (17), 2562−2571.
(48) Chiefari, J.; Chong, Y. K.; Ercole, F.; Krstina, J.; Jeffery, J.; Le, T. P. T.; Mayadunne, R. T. A.; Meijs, G. F.; Moad, C. L.; Moad, G.; Rizzardo, E.; Thang, S. H. Living Free-Radical Polymerization by Reversible Addition-Fragmentation Chain Transfer: The RAFT Process. *Macromolecules* **1998**, *31* (16), 5559−5562.
(49) Perrier, S. 50th Anniversary Perspective: RAFT Polymerization - A User Guide. *Macromolecules* **2017**, *50* (19), 7433−7447.

https://doi.org/10.1021/acsami.3c14859
ACS Appl. Mater. Interfaces 2023, 15, 58917−58930

(50) Khodabandeh, A.; Dario Arrua, R.; Desire, C. T.; Rodemann, T.; Bon, S. A. F.; Thickett, S. C.; Hilder, E. F. Preparation of Inverse Polymerized High Internal Phase Emulsions Using an Amphiphilic Macro-RAFT Agent as Sole Stabilizer. *Polym. Chem.* **2016**, *7* (9), 1803−1812.
(51) Luo, Y.; Wang, A. N.; Gao, X. One-Pot Interfacial Polymerization to Prepare PolyHIPEs with Functional Surface. *Colloid Polym. Sci.* **2015**, *293* (6), 1767−1779.
(52) Wang, Y.; Wan, X.; He, J.; Azhar, U.; Chen, H.; Zhao, J.; Pang, A.-m.; Geng, B. A One-Step Fabrication and Modification of HIPE-Templated Fluoro-Porous Polymer Using PEG-b-PHFBMA Macro-surfactant. *J. Mater. Sci.* **2020**, *55* (12), 4970−4986.
(53) Mathieu, K.; Jérôme, C.; Debuigne, A. Influence of the Macromolecular Surfactant Features and Reactivity on Morphology and Surface Properties of Emulsion-Templated Porous Polymers. *Macromolecules* **2015**, *48* (18), 6489−6498.
(54) Zhang, T.; Silverstein, M. S. Microphase-Separated Macroporous Polymers from an Emulsion-Templated Reactive Triblock Copolymer. *Macromolecules* **2018**, *51* (10), 3828−3835.
(55) Viswanathan, P.; Johnson, D. W.; Hurley, C.; Cameron, N. R.; Battaglia, G. 3D Surface Functionalization of Emulsion-Templated Polymeric Foams. *Macromolecules* **2014**, *47* (20), 7091−7098.
(56) Viswanathan, P.; Chirasatitsin, S.; Ngamkham, K.; Engler, A. J.; Battaglia, G. Cell Instructive Microporous Scaffolds through Interface Engineering. *J. Am. Chem. Soc.* **2012**, *134* (49), 20103−20109.
(57) Horowitz, R.; Lamson, M.; Cohen, O.; Fu, T. B.; Cuthbert, J.; Matyjaszewski, K.; Silverstein, M. S. Highly Efficient and Tunable Miktoarm Stars for HIPE Stabilization and PolyHIPE Synthesis. *Polymer* **2021**, *217*, 123444.
(58) Zhang, T.; Gui, H.; Xu, Z.; Zhao, Y. Hydrophobic Polyurethane PolyHIPEs Templated from Mannitol within Nonaqueous High Internal Phase Emulsions for Oil Spill Recovery. *J. Polym. Sci., Part A: Polym. Chem.* **2019**, *57* (12), 1315−1321.
(59) Berezovska, I.; Kapilov, K.; Dhavalikar, P.; Cosgriff-Hernandez, E.; Silverstein, M. S. Reactive Surfactants for Achieving Open-Cell PolyHIPE Foams from Pickering Emulsions. *Macromol. Mater. Eng.* **2021**, *306* (6), 2000825.
(60) Nicolaÿ, R. Synthesis of Well-Defined Polythiol Copolymers by RAFT Polymerization. *Macromolecules* **2012**, *45* (2), 821−827.
(61) Le Neindre, M.; Magny, B.; Nicolaÿ, R. Evaluation of Thiocarbonyl and Thioester Moieties as Thiol Protecting Groups for Controlled Radical Polymerization. *Polym. Chem.* **2013**, *4* (22), 5577−5584.
(62) Lai, J. T.; Filla, D.; Shea, R. Functional Polymers from Novel Carboxyl-Terminated Trithiocarbonates as Highly Efficient RAFT Agents. *Macromolecules* **2002**, *35* (18), 6754−6756.
(63) Pavlović, D.; Lou, Q.; Linhardt, J. G.; Künzler, J. F.; Shipp, D. A. Poly(N-Vinylpyrrolidone)-Polydimethylsiloxane Amphiphilic ABA Triblock Copolymers. *J. Polym. Sci., Part A: Polym. Chem.* **2017**, *55* (20), 3387−3394.
(64) Perera, M. M.; Ayres, N. Gelatin Based Dynamic Hydrogels via Thiol-Norbornene Reactions. *Polym. Chem.* **2017**, *8* (44), 6741−6749.
(65) Carnachan, R. J.; Bokhari, M.; Przyborski, S. A.; Cameron, N. R. Tailoring the Morphology of Emulsion-Templated Porous Polymers. *Soft Matter* **2006**, *2* (7), 608−616.
(66) Keane, D. P.; Mellor, M. D.; Poling-Skutvik, R. Responsive Telechelic Block Copolymers for Enhancing the Elasticity of Nanoemulsions. *ACS Appl. Nano Mater.* **2022**, *5*, 5934−5943.
(67) Sarraguça, J. M. G.; Pais, A. A. C. C.; Linse, P. Influence of Droplet Properties on the Formation of Microemulsion-ABA-Triblock Copolymer Networks. *Soft Matter* **2009**, *5* (1), 140−147.
(68) Sun, G.; Liu, M.; Zhou, X.; Hong, L.; Ngai, T. Influence of Asymmetric Ratio of Amphiphilic Diblock Copolymers on One-Step Formation and Stability of Multiple Emulsions. *Colloids Surf.* **2014**, *454* (1), 16−22.
(69) Wood, A. B. *Textbook of Sound*; G. Bell & Sons: London, 1949.
(70) Kuster, G. T.; Toksöz, M. N. Velosity and Attenuation of Seismic Waves in Two-Phase Media: Part I. Theoretical Formulations. *Geophysics* **1974**, *39* (5), 587−737.

https://doi.org/10.1021/acsami.3c14859
ACS Appl. Mater. Interfaces 2023, 15, 58917−58930